JOURNAL OF Materials CHEMISTRY

Electrochemical lithium insertion in a cation deficient thiospinel $Cu_{3.31}GeFe_4Sn_{12}S_{32}$

C. Bousquet,[a] C. Pérez Vicente,[a] A. Krämer,[a] J. L. Tirado,[b] J. Olivier-Fourcade and J. C. Jumas*[a]

[a] *Laboratoire de Physicochimie de la Matière Condensée (UMR 5617 CNRS), CC-003, Université Montpellier II, Place Eugène Bataillon, 34095 Montpellier Cedex 5, France*

[b] *Laboratorio de Química Inorgánica, Facultad de Ciencias, Universidad de Córdoba, Avda. San Alberto Magno, s/n, 14004 Córdoba, Spain*

We present the characterization and the electrochemical study of the cation deficient thiospinel $Cu_{3.31}GeFe_4Sn_{12}S_{32}$ as a cathodic material in lithium cells. The pristine compound has a spinel-related structure, where the copper defect in the tetrahedral site induces a partial oxidation of Fe^{II} to Fe^{III}. The discharge curve shows the presence of several insertion steps. The reduction of Fe^{III} to Fe^{II} and a copper extraction takes place during the first and second steps, respectively. Moreover, the lithium insertion originates a first-order spinel to rocksalt transition, indicated by the third step of the discharge curve. Finally, at low voltages (<1.65 V) a Sn^{IV} to Sn^{II} reduction takes place.

Introduction

Spinel-related structure compounds AB_2X_4 (space group $Fd\bar{3}m$) are three-dimensional lattices owing to the presence of a rigid framework of BX_6 octahedra and AX_4 tetrahedra. The structure can be described as a cubic close-packing arrangement of X anions (in 32e sites), B cations in hexacoordinated 16d sites and A cations in tetracoordinated 8a sites. Half of the octahedral sites (16c) and 7/8 of the tetrahedral sites (8b and 48f) defined by the packing of X atoms are empty. The vacancies are interconnected and provide a large number of theoretically available sites for intercalation reactions.

Since the work of Eisenberg[1] showing that lithium can be reversibly inserted into some copper, nickel and cobalt thiospinels, chalcogenide spinels have been extensively studied as host lattices. The effect of the lithium insertion in oxide compounds with the spinel structure was first described by Thackeray *et al.*[2] The B_2X_4 framework remains intact during the insertion reaction, while A cations are displaced to the initially empty 16c sites due to the electrostatic repulsion between A cations and the inserted lithium ions in the 16c sites. This migration of A cations is at the origin of the spinel to rocksalt first-order transition.

In the thiospinels, the diffusion path of lithium ions can be improved by removing A cations from the spinel structure. This is the case for the example of copper extraction carried out by treatment with mild oxidizing agents first reported in $CuTi_2S_4$.[3,4] Also, treatment with a large excess of *n*-butyllithium results in the extraction of copper ions as Cu^0. The electrochemical behavior of the cation deficient solids in lithium cells improved significantly.[5–7] For these compounds, a topotactic lithium insertion was observed when the number of A site cation vacancies inhibited the spinel to rocksalt first-order transition. The lithium mobility in these defect spinels is higher, owing to larger bottlenecks between 8a tetrahedra and 16c octahedra than in spinel compounds with filled 8a sites.[5–8]

Recently[9] lithium insertion in $Cu_2MSn_3S_8$ (M = Mn, Fe, Co, Ni) has been reported. In order to improve the electrochemical performance, by the presence of vacancies in the tetrahedral 8a site, copper extraction with I_2/CH_3CN was carried out. In this work, we study the cation deficient spinel $(Cu_{3.31}Ge\square_{3.69})_{8a}[Fe_4Sn_{12}]_{16d}S_{32}$, where the vacancies in the tetrahedral 8a sites result from a topotactic substitution of four Cu^I by one Ge^{IV},which is accompanied by the generation of Cu deficiency to yield more than three vacancies in the 8a sites. The insertion behavior of this new Ge-containing material is compared with that previously described in the products resulting from copper extraction.

Experimental

$Cu_{3.31}GeFe_4Sn_{12}S_{32}$ was synthesized from the pure elements, which were mixed and sealed in evacuated ($P<10^{-5}$ mm Hg) quartz tubes. The mixtures were heated at 250 °C, at 50 °C h^{-1}. This temperature was kept constant for 48 h. Then the temperature was increased to 680 °C for 7 days. The product was ground and stored in an argon-filled glove-box.

The electrochemical lithium insertion was carried out in two-electrode cells. The cathode was prepared from the pure compound. Pellets of diameter 7 mm were obtained by pressing 20–30 mg of powder at 1.5 ton cm^{-2}. The anode was a metallic lithium disk. The electrolyte was 1 M $LiClO_4$ in polypropylene-carbonate, supported by a glass-paper disk. The discharge curve was obtained at room temperature with a multichannel microprocessor-controlled system (MacPile). An initial relaxation was allowed until $\Delta V/\Delta t$ was lower than 1 mV h^{-1}. The current density during the discharge was 50 μA cm^{-2}. The average lithium content was calculated from the amount of electron charge transferred to the cathode, on the assumption that no current was due to side reactions.

Mössbauer spectra of the samples were obtained at room temperature with an ELSCINT AME 40 constant acceleration spectrometer. The sources were ^{119m}Sn in a $BaSnO_3$ matrix and ^{57}Co in a Rh matrix for ^{119}Sn and ^{57}Fe spectra respectively. The velocity scale was calibrated by using a ^{57}Co source and the magnetic sextet spectrum of a high purity iron foil absorber. Recorded spectra were fitted to Lorentzian profiles by least squares method[10] and the fit quality was controlled by the classical χ^2 method. The origin of the isomer shift of ^{119}Sn and ^{57}Fe spectra was determined from the center of the $BaSnO_3$ and α-Fe spectra, also recorded at room temperature.

X-Ray powder diffraction (XRD) patterns were recorded on a Philips diffractometer using Cu-Kα radiation. In order to avoid the oxidation reactions of the lithiated products during the recording of the XRD patterns, the samples were covered with a thin parafilm. For analyzing the structural modifications induced by the intercalation process, Rietveld analyses of XRD patterns were carried out, with the aid of the computer program Rietveld Analysis Program DBWS-9411.[11]

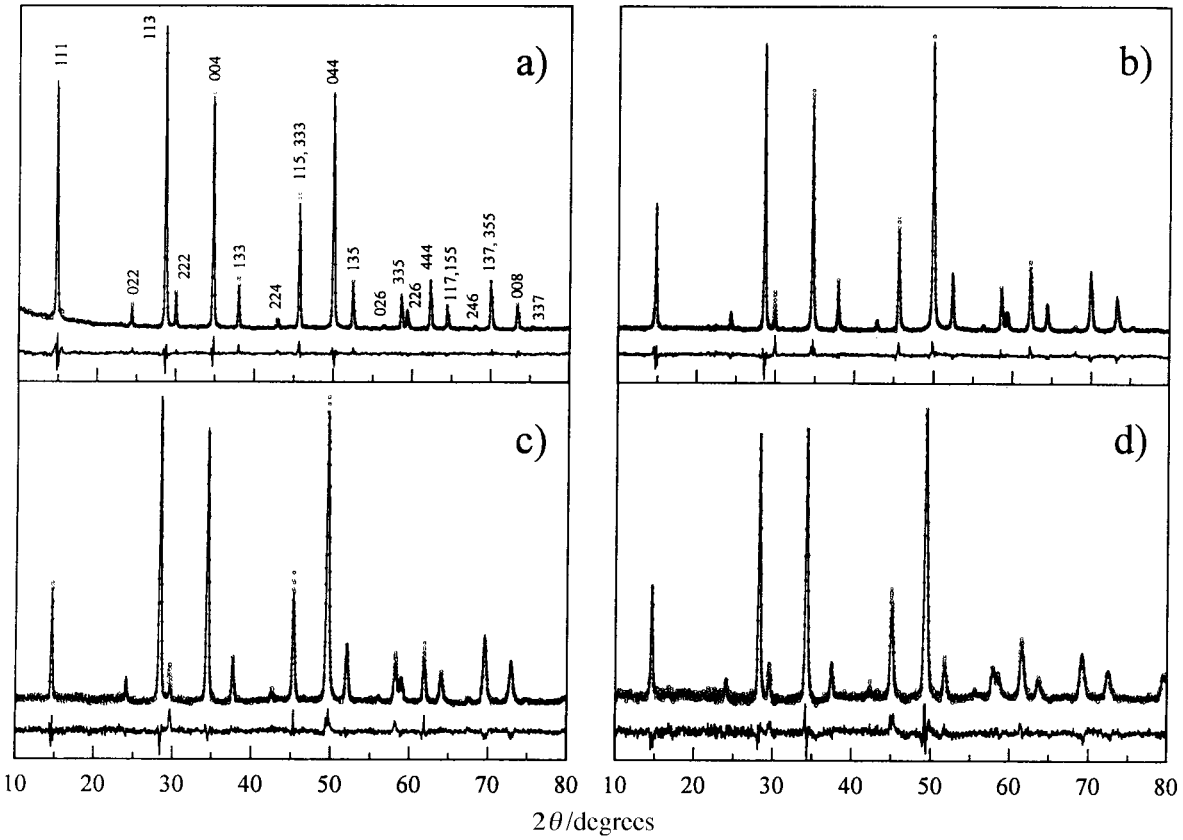

Fig. 1 X-Ray diffraction patterns and Rietveld analyses of $Li_xCu_{3.31}GeFe_4Sn_{12}S_{32}$ at $x=0$ (a), $x=2$ (b), $x=4$ (c) and $x=6$ (d)

Results and Discussion

Fig. 1 shows the X-ray diffraction pattern of the pristine compound, $Cu_{3.31}GeFe_4Sn_{12}S_{32}$, the Rietveld refinement and the difference between them. Table 1 includes the refined parameters. The cubic unit cell parameter, 10.338 Å, is slightly higher than that reported for $Cu_8Sn_{12}Fe_4S_{32}$, 10.312 Å.[8] Thus, the substitution of Cu by Ge and the presence of vacancies in tetrahedral sites (discussed below) slightly modify the spinel framework. On the other hand, the substitution of four Cu atoms by one Ge atom could take place by retaining four Cu atoms per unit cell. Under these conditions, the oxidation state of all the atoms present and the electroneutrality of the solid can be maintained. However, the results of the Rietveld analysis are indicative of an additional effect, which leads to a deficiency of Cu atoms. Thus, the occupancy of 8a sites by copper is reduced to 3.31. This in turn can take place only if the formal oxidation states of some cations increase, in order to retain electroneutrality. If an oxidation number of four is assumed for both Sn and Ge, only two options are possible: the presence of 0.69 Cu^{II} or Fe^{III} instead of the theoretical oxidation states Cu^{I} and Fe^{II}. It is well known that the Mössbauer spectrum can help to identify the presence or absence of Fe^{III} which would indicate which of these two options takes place. Unfortunately, some complications are present in the spectra of the $Cu_{3.31}GeFe_4Sn_{12}S_{32}$ spinel compound. For Fe^{II} two different electron configurations are possible: low spin (LS, 3d t_{2g}^6) and high spin (HS, 3d $t_{2g}^4\ e_g^2$). At very low temperature, the time that iron spends in the HS or LS state is much longer than the mean lifetime of the excited ^{57}Fe Mössbauer state,

Table 1 Results of the Rietveld analysis of XRD patterns of $Li_xCu_{3.31}GeSn_{12}Fe_4S_{32}$ at different discharge depths, according to the $Fd\bar{3}m$ space group, origin 2

		occupancy					correlation factors	
	site	Cu	Ge	Sn	Fe	S		
0 Li/mol	8a (T_d)	3.31(6)	1.00	—	—		R_{WP}	8.44
[$a=10.338(1)$ Å,	16d (O_h)	—	—	12.00	4.00		S	1.46
$x^a=0.2556(2)$]	32e	—	—	—	—	32.00	R_{Bragg}	3.87
2 Li/mol	8a (T_d)	1.88(3)	1.00	—	2.16(5)	—	R_{WP}	10.48
[$a=10.335(1)$ Å,	16d (O_h)	—	—	12.00	1.84(5)	—	S	1.77
$x=0.2515(2)$]	32e	—	—	—	—	32.00	R_{Bragg}	5.62
4 Li/mol	8a (T_d)	0.92(3)	1.00	—	3.15(3)	—	R_{WP}	11.56
[$a=10.351(2)$ Å,	16d (O_h)	—	—	12.00	0.85(3)	—	S	2.42
$x=0.2522(2)$]	32e	—	—	—	—	32.00	R_{Bragg}	5.45
6 Li/mol	8a (T_d)	0.90(5)	1.00	—	2.45(5)	—	R_{WP}	12.96
[$a=10.390(3)$ Å,	16c (O_h)	—	—	—	1.55(5)	—	S	3.04
$x=0.2511(2)$]	16d (O_h)	—	—	12.00	—	—	R_{Bragg}	5.58
	32e	—	—	—	—	32.00		

[a] x = Sulfur position.

and both HS and LS states can be clearly identified, as well as the presence of Fe^{III}. In contrast, at room temperature, the lifetimes of the HS and LS states become comparable to the lifetime of the Mössbauer transition. Thus, HS↔LS transitions take place during the excited Mössbauer state and a typical relaxation spectrum is obtained. This behavior has been described in detail by Womes *et al.*[12] For the $Cu_8Fe_4Sn_{12}S_{32}$ phase, the RT spectrum is composed of two peaks centered at *ca.* 0.2 and 1.3 mm s^{-1}, the first one being more intense and narrower than the second one.[9,12] After Cu extraction, a new effect appears between both peaks.[9] A simplified treatment of the ^{57}Fe Mössbauer spectrum was reported for the copper deficient compound with $Cu_{8-x}Fe_4Sn_{12}S_{32}$ stoichiometry. The decrease of the isomer shift and quadrupole splitting after Cu extraction has been attributed to a slight reduction of the screening effect caused by the loss of d electrons, and is therefore ascribable to a partial oxidation of Fe^{II} to Fe^{III}. Fig. 2 shows the ^{57}Fe Mössbauer spectra of $Cu_8Fe_4Sn_{12}S_{32}$ and the copper deficient thiospinel $Cu_{3.31}GeFe_4Sn_{12}S_{32}$. A decrease of the isomer shift and the presence of the same effect between both theoretical peaks are observed, in a similar way to the phase $Cu_{8-x}Fe_4Sn_{12}S_{32}$ after copper extraction. Thus, by comparison of the two Cu deficient compounds, we can conclude that the Cu defect in $Cu_{3.31}GeFe_4Sn_{12}S_{32}$ induces $Fe^{II}\rightarrow Fe^{III}$ oxidation. However, the separate contributions of Fe^{III} and Fe^{II} to the profile are not clearly resolved, probably due to a fast electron transfer between Fe^{II} and Fe^{III}, which makes them non-distinguishable atoms in the spinel structure.

Additional information can be obtained from the ^{119}Sn Mössbauer spectrum, shown in Fig. 3. The hyperfine parameters are included in Table 2. The values of the isomer shift and quadrupole splitting are characteristic of Sn^{IV} in a slightly distorted octahedral coordination. A decrease of the isomer shift is observed after the substitution Ge/Cu. From these data, it is evident that this substitution and the presence of vacancies make the covalent character of the Sn—S bond decrease. This effect is probably due to the high polarization power of Ge^{IV} which attracts the electronic density from S anions resulting in a decrease of the electronic density at the Sn—S bond and an increase of its ionic character. This result contrasts with the behavior observed in chemically deintercalated $Cu_{8-x}Fe_4Sn_{12}S_{32}$, where a very slight increase of the isomer shift was interpreted as due to a small increase in the covalent character of the Sn—S bonding.[9] The sign of the changes induced in bond character is different for each procedure used in the generation of 8a site vacancies, and this may lead to significant differences in the intercalation behavior, as shown below.

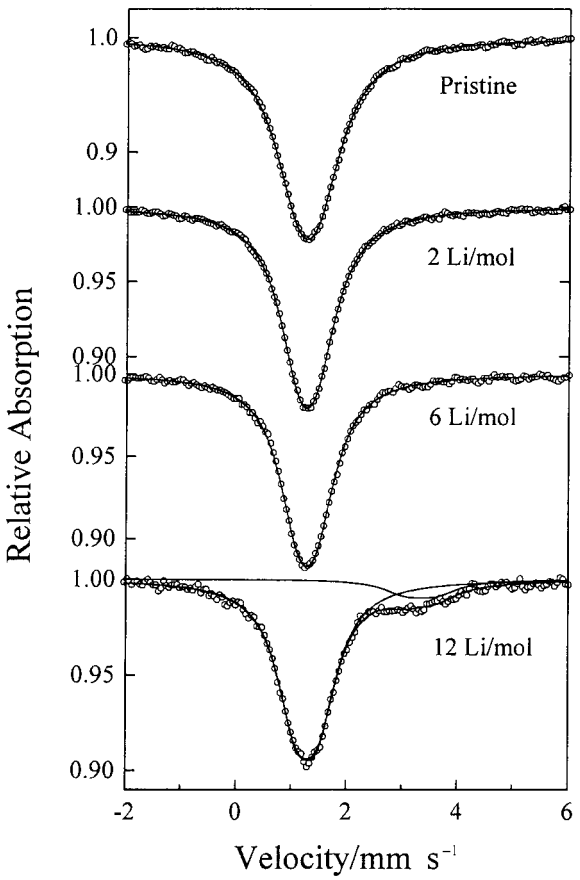

Fig. 3 ^{119}Sn Mössbauer spectra recorded at room temperature of $Li_xCu_{3.31}GeFe_4Sn_{12}S_{32}$ at different lithium contents

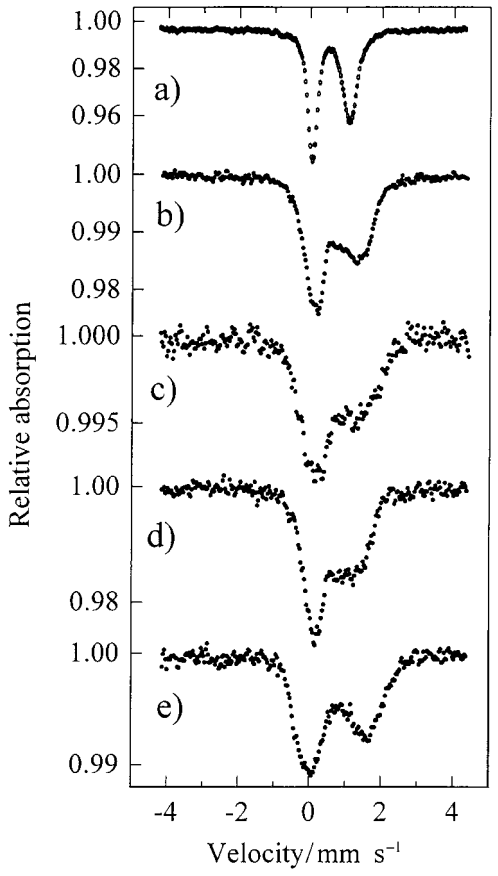

Fig. 2 ^{57}Fe Mössbauer spectra recorded at room temperature of $Cu_8Fe_4Sn_{12}S_{32}$ (from ref. 12) (a), pristine $Cu_{3.31}GeFe_4Sn_{12}S_{32}$ (b); and lithiated $Li_xCu_{3.31}GeFe_4Sn_{12}S_{32}$ at $x=2$ (c), $x=6$ (d) and $x=12$ (e)

On the other hand, the increase of the linewidth in the ^{119}Sn spectra of $Cu_{3.31}GeFe_4Sn_{12}S_{32}$ as compared with $Cu_8Fe_4Sn_{12}S_{32}$ is similar in sign and slightly larger than that found in $Cu_{8-y}Fe_4Sn_{12}S_{32}$. In both cation deficient solids, the enhanced broadening is in good agreement with the presence of slightly different Sn^{IV} environments. While in $Cu_{8-y}Fe_4Sn_{12}S_{32}$, all the tetrahedral neighbors are Cu atoms, Cu atoms and vacancies are possible in $Cu_{8-y}Fe_4Sn_{12}S_{32}$ and three different neighbors are present in our compound $Cu_{3.31}GeFe_4Sn_{12}S_{32}$: Cu, Ge and vacancies. The statistical distribution of these three neighbors means that the environments of all Sn^{IV} are slightly different, having as a final effect an increase of the linewidth of the peak.

Fig. 4 shows the continuous galvanostatic discharge and the incremental capacity of $Cu_{3.31}GeFe_4Sn_{12}S_{32}$ as a cathodic material. It is characterized by three regions of nearly constant voltage or steps centered at *ca.* 0.20, 1.73 and 5.02 Li/mol. A fourth step appears for larger discharge depths. The four regions observed in the discharge curve of Fig. 4(a) are regions of weak but non-zero slope which lead to measurable peaks

Table 2 Hyperfine parameters of ^{119}Sn Mössbauer spectra of $Cu_2FeSn_3S_8$ and $Li_xCu_{3.31}GeFe_4Sn_{12}S_{32}$ at different x values: isomer shift (δ), quadrupole splitting (Δ) and full-width at half-maximum (Γ)

compound	composition (x)	δ/mm s^{-1}	Δ/mm s^{-1}	Γ/mm s^{-1}	attribution
$Cu_2FeSn_3S_8$[a]	—	1.246(1)	0.321(6)	0.863(6)	Sn^{IV}
$Cu_{1.8}FeSn_3S_8$[a]	—	1.275(1)	0.321(9)	0.924(8)	Sn^{IV}
$Li_xCu_{3.31}GeFe_4Sn_{12}S_{32}$	0	1.177(5)	0.36(1)	1.126(9)	Sn^{IV}
	2	1.181(5)	0.309(9)	0.949(8)	Sn^{IV}
	6	1.185(5)	0.33(1)	0.89(1)	Sn^{IV}
	12	3.25(5)	0.55(8)	0.9(1)	Sn^{II}(11%)
		1.196(6)	0.41(1)	0.86(2)	Sn^{IV}(89%)

[a]From ref. 9.

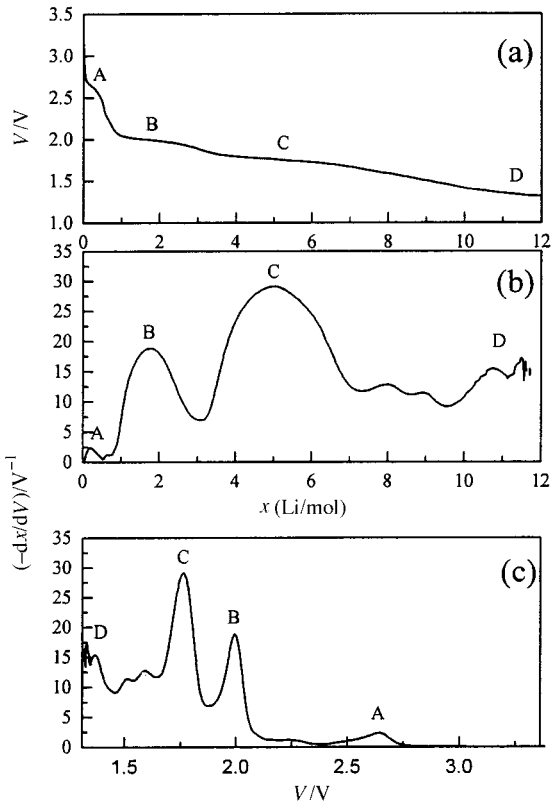

Fig. 4 Discharge curve (a) and incremental capacity as a function of x (b) and V (c) using $Cu_{3.31}GeFe_4Sn_{12}S_{32}$ as cathodic material and Li as anode

in the incremental capacity plots of Fig. 4(b) and (c). These effects can be associated to different steps of electron plus lithium injection. Such steps can be associated to single-phase processes (confirmed by X-ray diffraction, where only one phase is present) in which the insertion of lithium probably takes place in different set of sites. Table 3 summarizes the position of the different regions. The first one (A in Fig. 4) extending from $x=0$ to $x=0.56$, can be attributed to the reduction of $Fe^{III}\rightarrow Fe^{II}$. This limiting value of x is close to that obtained from Rietveld, 0.69. This step has also been observed for the phase $Cu_{8-y}Sn_{12}M_4S_{32}$ (M = Fe, Co),[9] where the vacancies have been created by treating the compound with an oxidizing agent (I_2/CH_3CN) to reach the value $y=0.64$ and $y=3.44$ for M = Fe and Co respectively. As explained above, it has been assumed that the copper extraction originates the change $M^{II}\rightarrow M^{III}$. Thus, this first step has also been attributed to $M^{III}\rightarrow M^{II}$ reduction.

In order to study the structural modification that occurs during the second step of the discharge curve of $Cu_{3.31}GeFe_4Sn_{12}S_{32}$ (B in Fig. 4), a sample with 2 Li/mol was produced and the XRD pattern analyzed [see Fig. 1(b)]. An increase of the intensity of the (044) reflection and a decrease of the (111) is observed. For the compound without vacancies, $Cu_8Fe_4Sn_{12}S_{32}$, a small region is also detected and it was attributed to a copper extraction.[9] However, this makes the (111) reflection increase; just the opposite effect is observed in our case. The classical first-order transition induced in the other system involves a 8a→16c migration, which also results in an increase of not only the (111) but also the (004) reflection. This simplified process does not describe accurately the results of the Rietveld refinements. A simulation shows that the observed effect on the intensities is a combination of two effects: an increase of population in tetrahedral sites and a decrease in octahedral ones. This can take place by a simple cation migration from 16d to 8a sites. The ^{119}Sn Mössbauer spectrum of this sample (Fig. 3) showed a single peak centered at 1.181 mm s^{-1}, the same value as for the pristine compound. This means that the local environment of tin atoms does not change. Because no additional peaks ascribable to Sn in tetrahedral coordination appear, we can assume that the migration 16d→8a only affects Fe atoms.

Additional data were obtained by recording the ^{57}Fe Mössbauer spectra, which are included in Fig. 2. A qualitative inspection of these spectra shows some significant changes in the experimental profiles. On increasing the depth of discharge, an increase in the linewidth and slight changes in the positions of the maxima are observed. These effects can be attributed to the coexistence of iron in different sites. Unfortunately, due to

Table 3 Limits and attribution of the different regions in the discharge curve of $Cu_{3.31}GeFe_4Sn_{12}S_{32}$

	voltage/V			composition (x)			
	limits		centered	limits		centered	
step	lower	upper	at	lower	upper	at	attribution
A	2.75	2.38	2.64	0.00	0.56	0.20	$Fe^{III}\rightarrow Fe^{II}$
B	2.38	1.88	1.99	0.56	3.07	1.73	$Cu^{I}\rightarrow Cu^{0}$ (s) accompanied by $Fe(O_h)\rightarrow Fe(T_d)$
C	1.88	1.65	1.76	3.07	7.33	5.02	spinel to rock-salt first order transition reduction?
D	1.65	—	—	7.33	—	—	$Sn^{IV}\rightarrow Sn^{II}$

the problem discussed above of the HS–LS transition, detailed quantitative analysis of the spectra can not be carried out. Thus, the Mössbauer spectra could not be used to confirm whether the new occupied sites are tetrahedral or octahedral.

Taking into account these data, the Rietveld refinement of the XRD pattern has been carried out. In a first time, only the iron distribution between 8a and 16d sites has been refined. Finally, the occupation factor of Cu atoms has also been refined, and the results are included in Table 1. From this Rietveld refinement, two effects are evident: first, a copper extraction, in a way similar to that which was observed for the compounds $Cu_{8-x}Fe_4Sn_{12}S_{32}$; second, an iron migration from 16d to 8a sites. Thus, the occupancy factor of the 16d sites decreases from 16 to 13.84 atoms and increases for the 8a sites from 4.31 to 5.04 atoms. As we discussed above, the presence of vacancies in the 8a sites (from 3.69 to 5.2 as copper is extruded during the discharge to 2 Li/mol) inhibits the spinel to rocksalt transition, probably because the inserted lithium atoms are not placed in the 16c sites but in the vacancies present in the 8a tetrahedral sites. In fact, due to the low scattering power of lithium atoms compared to the other atoms present in the structure of the thiospinel studied, location of lithium atoms is difficult. Nevertheless, indirect measurements may give additional proof of lithium site occupancy. According to James *et al.*[5,6] the smooth variation found in the OCV curves of $Li/Cu_{0.07}Ti_2S_4$ and $Li/Cu_{0.05}Zr_2S_4$ cells, with no discontinuity at the normal spinel compositions $Li_{0.93}Cu_{0.07}Ti_2S_4$ and $Li_{0.95}Cu_{0.05}Zr_2S_4$, imply that the inserted lithium occupies only the 16c octahedral sites at all compositions. This was later confirmed by powder neutron diffraction. In our case, for $Cu_{3.31}GeFe_4Sn_{12}S_{32}$, the normal spinel composition is reached at $x=3.69$ in $Li_xCu_{3.31}GeFe_4Sn_{12}S_{32}$. The discharge curve of the lithium cell reveals a second effect which ends at $x=3.07$. Having in mind the possible deviations from the strict thermodynamic equilibrium and the changes in Fe occupancy, this limit could be indicative of Li 8a site occupancy during the first steps of the discharge.

To analyze the third step (C in Fig. 4), two lithiated samples have been obtained at 4 and 6 Li/mol. The refined X-ray diffraction patterns are included in Fig. 1(c) and (d) and the obtained values are in Table 1. It is worth noting that not all the Cu atoms have been extracted during the second step of the discharge, remaining at 0.92 in the tetrahedral sites. Thus, the total amount of copper extracted as Cu^0 is 2.39. This value is similar to the Δx value resulting from the extension of the second region. It extends from 0.56 to 3.07 Li/mol, which corresponds to $\Delta x=2.51$. At this discharge depth, the migration of Fe atoms from 16d to 8a sites occurs. Moreover, a slight increase of the lattice parameter is observed. This expansion is also observed for the sample obtained at 6 Li/mol. The lithium content is close to the theoretical vacancy content. Thus, after reaching the composition of a normal spinel, lithium atoms are probably inserted into the 16c octahedral sites. This is the origin of the spinel to rocksalt first-order transition.[2] This fact is confirmed by the Rietveld analysis: a migration of Fe atoms from the 8a sites towards 16c sites is observed. The ^{57}Fe Mössbauer spectrum at $x=6$ again shows a complex profile. It will be analyzed in the light of the observations for $x=12$. Furthermore, the ^{119}Sn Mössbauer spectrum (Fig. 3) shows a single peak with an isomer shift characteristic of Sn^{IV}. There is not a clear reduction $Sn^{IV}\rightarrow Sn^{II}$ since no additional peak ascribable to Sn^{II} was observed. Concerning Cu atoms, no additional extraction process was noted, confirming that the copper reduction $Cu^{I}\rightarrow Cu^0$ takes place only during the second step on the discharge curve.

During the insertion processes, a progressive amorphization of the lithiated product takes place. A general decrease of the intensity of the peaks is observed, clearly indicated by an increase of the relative background intensity. This effect can be observed from the plots of the difference between the experimental and refined X-ray diffraction patterns in Fig. 1. Also the correlation parameters of the Rietveld refinement suggest this amorphization. So, while the value of R_{Bragg} (which takes into account only the intensity of the Bragg reflections) is about 5.5% for the samples with 2, 4 and 6 Li/mol, an increase of R_{wp} and R_{wp}/R_{exp} is obtained, due to the relative increase of the background. An increase of the linewidth also takes place. Because of this amorphization process a good Rietveld refinement is not possible for higher lithium contents. Fig. 5 shows the XRD patterns of the samples obtained at 8 and 12 Li/mol, where the poor crystallinity of the product is evident. However, a value of the lattice parameter can be derived. Fig. 6 shows the evolution of the unit cell parameter as a function of the lithium content. For low x values, when lithium insertion is accompanied by copper extraction, no expansion of the lattice is observed. On the other hand, when this Cu extraction is stopped and can not compensate for the effect of the lithium insertion, an expansion of the lattice takes place. This expansion is not very important at 4 Li/mol, probably because vacancies are already present to accommo-

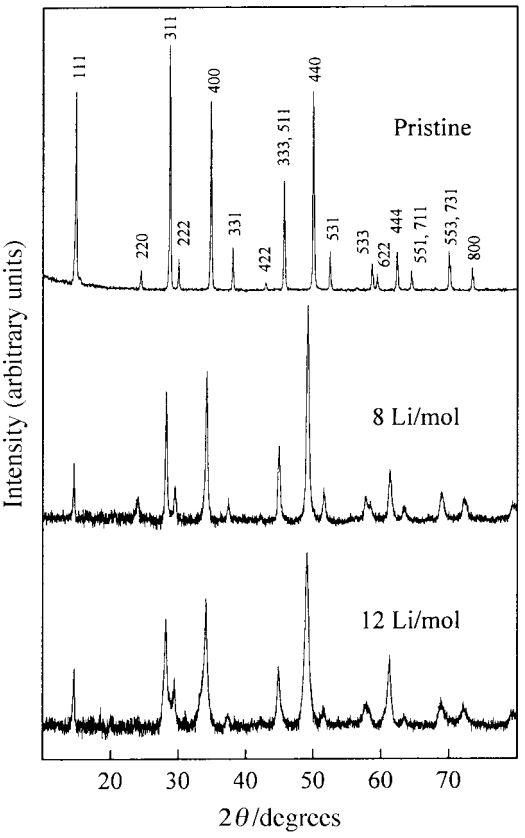

Fig. 5 X-Ray diffraction patterns of pristine and lithiated compounds (at $x=8$ and 12)

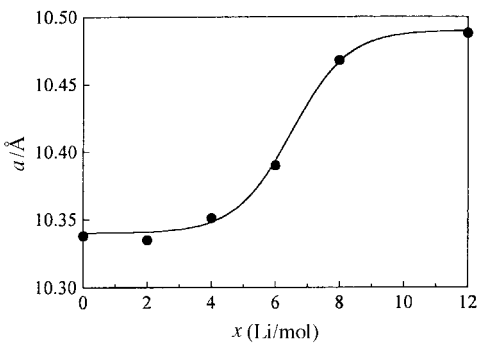

Fig. 6 Evolution for the unit cell parameter of $Li_xCu_{3.31}GeFe_4Sn_{12}S_{32}$ as a function of the lithium content

date inserted lithium ions. At 6 Li/mol, when the system is at the beginning of the spinel to rocksalt transition, an important expansion takes place, a phenomenon that is also present at 8 Li/mol. For higher lithium contents (12 Li/mol) only a slight expansion is observed, probably because the expansion of the lattice is large enough to accommodate the inserted lithium. It should be noted that the expansion in a spinel lattice is always restricted, due to the rigidity of the framework. Thus, the evolution of the unit cell parameter shown in Fig. 6 is particularly significant.

Concerning the cation distribution, at 8 Li/mol the presence of the (220) Bragg reflection indicates that the transition to the rocksalt structure is not yet complete, since this reflection is especially sensitive to the occupation factor of tetrahedral sites. In contrast, at 12 Li/mol, this reflection is not present, and the migration from 8a to 16c sites has been completed. The (111) spinel reflection is always present, probably due to a different occupancy of octahedral 16d and 16c sites. The ^{57}Fe Mössbauer spectrum [Fig. 2(e)] agrees well with this situation and only the two peaks of the relaxation spectrum are observed. The profile of this spectrum is close to that of $Cu_8Fe_4Sn_{12}S_{32}$, where Fe^{II} cations occupy the octahedral 16d sites. The comparison with our sample at $x=12$ shows an important increase of the linewidth. This phenomenon can be attributed to two effects: first, the presence of two different octahedral environments (16c and 16d) which are not exactly equivalent; second, an amorphization process, creating a strong distortion of the coordination polyhedra. Thus, the ^{57}Fe Mössbauer spectrum at $x=6$ [Fig. 2(d)] corresponds to a transition state between the cation distribution present before and after the spinel to rocksalt transition.

Finally, the ^{119}Sn Mössbauer spectrum at 12 Li/mol (see Fig. 3) presents two peaks, ascribable to Sn^{IV} and Sn^{II} in octahedral coordination, indicating that step D in Fig. 4 can be attributed to Sn reduction. The hyperfine parameters are included in Table 2. In order to confirm the assignment of this step, a comparison with the discharge curve of $Cu_2FeSn_3S_8$[13] was carried out. In this case, only one step was detected, centered at 1.25 V. After substitution of Sn by Ti, to yield $Cu_2FeTi_3S_8$, a reduction region centered at 0.7 V appeared instead of the other one at 1.25 V. This confirms that step D in Fig. 4 can be attributed to $Sn^{IV}\rightarrow Sn^{II}$ reduction, while steps A, B and C in Fig. 4 are due to the presence of Fe^{III}, Ge and/or vacancies, effects that are not present in $Cu_2FeSn_3S_8$.

Conclusions

Ge/Cu substitution in the compound $Cu_8Fe_3Sn_{12}S_{32}$ has been carried out, accompanied by a copper defect to yield $Cu_{3.31}GeFe_4Sn_{12}S_{32}$ with the presence of 3.69 vacancies in the 8a sites. The copper defect induces the presence of Fe^{III}, to retain electroneutrality. The study of the electrochemical lithium insertion allowed us to identify the presence of four regions or steps. The first one, centered at 2.64 V, is attributed to the reduction $Fe^{III}\rightarrow Fe^{II}$. During the step at *ca.* 2 V, copper extraction takes place at the same time as iron migration from the octahedral 16d sites to the tetrahedral 8a sites. The X-ray diffraction patterns show that during the third step a first-order spinel to rocksalt transition takes place, but no reduction processes are observed. Finally, a fourth step was identified, corresponding to the reduction $Sn^{IV}\rightarrow Sn^{II}$, as indicated by ^{119}Sn Mössbauer spectroscopy results.

The authors are indebted to the European Community, the Ministries of Foreign Office (France) and Education (Spain) for the financial supports (JOU2-CT93-026 contract, Human Capital and Mobility no. ERBCHBGCT 93.0430, Training and Mobility of Researchers no. ERBFMBICT 96.0768 and PICASSO program).

References

1 M. Eisenberg, J. *Electrochem. Soc*., 1980, **127**, 2382.
2 M. M. Thackeray, W. I. F. David and J. B. Goodenough, *Mater. Res. Bull*., 1982, **17**, 785.
3 R. Schöllhorn and A. Payer, *Angew. Chem., Int. Ed. Engl*., 1985, **24**, 67.
4 S. Sinha and D. W. Murphy, *Solid State Ionics*, 1986, **20**, 81.
5 A. C. W. P. James, J. B. Goodenough, N. J. Clayden and P. M. Banks, *Mater. Res. Bull*., 1989, **24**, 143.
6 A. C. W. P. James, B. Ellis and J. B. Goodenough, *Solid State Ionics*, 1988, **27**, 45.
7 N. Imanishi, K. Inoue, Y. Takeda and O. Yamamoto, *J. Power Sources*, 1993, **43–44**, 1993.
8 P. de la Mora and J. B. Goodenough, *J. Solid State Chem*., 1987, **70**, 121.
9 P. Lavela, J. L. Tirado, J. Morales, J. Olivier-Fourcade and J. C. Jumas, *J. Mater. Chem*., 1996, **6**, 41.
10 K. Ruebenbauer and T. Birchall, *Hyperfine Interact*., 1979, **7**, 125.
11 D. B. Wiles and R. A. Young, *J. Appl. Crystallogr*., 1995, **28**, 366.
12 M. Womes, J. C. Jumas, J. Olivier-Fourcade, F. Aubertin and U. Gonser, *Chem. Phys. Lett*., 1993, **201**, 555.
13 C. Branci, J. Sarradin, J. Olivier-Fourcade and J. C. Jumas, *Mol. Cryst. Liq. Cryst*., in press.

Paper 8/02664E; *Received* 7*th April*, 1998